

Study of timing characteristics of a 3 m long plastic scintillator counter using waveform digitizers

A. Blondel^a, D. Breton^b, A. Dubreuil^a, A. Khotyantsev^c, A. Korzenev^{a,*}, J. Maalmi^b,
A. Mefodev^c, P. Mermod^{a, **}, E. Noah^a

^a*DPNC, Section de Physique, Université de Genève, Geneva, Switzerland*

^b*Laboratoire de L'accélérateur Linéaire from CNRS/IN2P3, Centre scientifique d'Orsay, France*

^c*Institute for Nuclear Research of the Russian Academy of Sciences, Moscow, Russia*

Abstract

A plastic scintillator bar with dimensions $3\text{ m} \times 2.5\text{ cm} \times 11\text{ cm}$ was exposed to a focused muon beam to study its light yield and timing characteristics as a function of position and angle of incidence. The scintillating light was read out at both ends by photomultiplier tubes whose pulse shapes were recorded by waveform digitizers. Results obtained with the WAVECATCHER and SAMPIC digitizers are analyzed and compared. A comprehensive discussion of the various factors affecting the timing resolution is presented. Prospects for applications of plastic scintillator technology in large-scale particle physics detectors with timing resolution around 100 ps are provided in light of the results.

Keywords: Scintillator, PMT, time resolution, digitiser, WAVECATCHER, SAMPIC, SHiP

1. Introduction

Plastic scintillator detectors have been extensively used in particle physics experiments since decades. In large-scale experiments, they typically represent an array of bars covering a large surface which can provide a fast trigger signal or particle identification using time-of-flight. Depending on the bar dimensions, scintillator type, and light readout sensor the time resolution for such detectors typically ranges from 50 ps (50 cm bars of the ToF system of MICE [1]) to 350 ps (6.8 m bars of the ToF system of OPAL [2]).

As a matter of actual practice, counters which are made of a bulk scintillator do not exceed 3 m in length. This restriction comes naturally from a signal attenuation and an uncer-

tainty related to the dispersion of photon path lengths which gets dominant for long counters. Moreover this uncertainty grows exponentially with a decrease of the thickness of a bar [3]. It makes a bar cross section close to a square shape advantageous in detectors [4, 5, 6, 7]. However, when a detector covers a large surface, for reasons of economy, the thickness of a counter along the beam is often chosen to be significantly smaller than its width. In this case the thickness becomes a limiting factor for the precision time measurement. Recent examples of detectors using this type of bars are the trigger hodoscopes system in COMPASS [8] and the NA61/SHINE ToF detector [9]. Another example of a detector which combines the requirements of a large covered surface and an excellent time resolution is the timing detector of the proposed SHiP experiment at the CERN SPS [10]. To efficiently distinguish between

*E-mail: alexander.korzenev@cern.ch

**E-mail: philippe.mermod@cern.ch

vertices from random muon crossings and genuine particle decays, the SHiP timing detector needs to cover a $6\text{ m} \times 12\text{ m}$ area with a time resolution of 100 ps or better [11] at an affordable price, which is a challenge. One option proposed in the SHiP technical proposal is an array of 3 m long plastic scintillator bars read out by photomultiplier tubes (PMTs) [11]. Another feature of SHiP is a software trigger running on an online computer farm, thus favoring the use of a DAQ electronics which has the particularity to tolerate relatively high event rates and at the same time allow for each channel to operate in a self-triggering mode.

Novel types of acquisition electronics which perform a waveform sampling using a switched capacitor array (SCA) are employed since recently in particle physics experiments. The use of an analog memory which is added in parallel with a delay line allows to sample an analog signal at very high rate. In addition, having the waveform recorded, one can extract various kinds of information like baseline, amplitude, charge and time. The measurements presented in this article with a 3 m bar were made with the two acquisition modules WAVECATCHER [12] and SAMPIC [13]. Both digitizers were used at the 3.2 GS/s sampling rate. The circular buffer of WAVECATCHER contains 1024 cells what makes possible to cover a 320 ns time window, thus to record the full signal coming from PMT. The WAVECATCHER measurements are therefore used as a reference. The SAMPIC, on the other hand, has a short buffer of 64 cells for a 20 ns window. Combined with an on-chip ADC, this allows though to work with rates two orders of magnitude higher than WAVECATCHER, making it attractive for applications such as the SHiP timing detector. The test-bench used here can thus be considered as a prototype for the conservative design of the timing detector of the SHiP experiment described in the technical proposal [11].

The article is organized as follows. The experimental setup is described in Section 2. Sec-

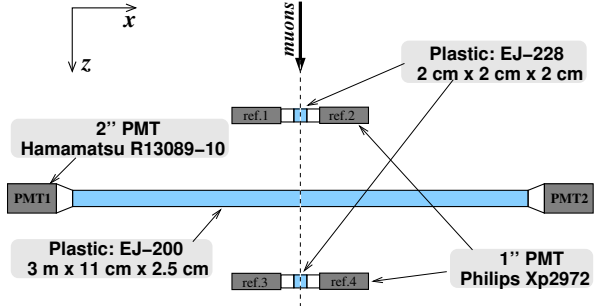


Figure 1: Schematic top view of the experimental setup. The outputs of all 6 PMTs are connected to a single acquisition module.

tion 3 provides a detailed description of the DAQ electronics. The analysis procedure is presented in Section 4. The results of the measurements are discussed in Section 5. Finally, a summary is given in Section 6.

2. Experimental setup

We present results of test-beam measurements which took place at the CERN PS in June 2016. The layout of the setup is shown in Fig. 1. The coordinate system is chosen such that the z axis is directed along the beam, the x axis is along the bar and the y axis is directed vertically in such a way that the coordinate system is right-handed. The origin of the system is at the left side of the bar, in the center of the cross section.

2.1. Plastic bar and PMTs

The scintillator counter has been purchased from the SCIONIX Radiation Detector & Crystals company [14]. The bar length is 3 m and its transverse cross section is $2.5\text{ cm} \times 11\text{ cm}$. The two larger surfaces of the bar ($3\text{ m} \times 11\text{ cm}$) were in contact with a casting form and had no other preparation. The four other surfaces were diamond milled. The choice of plastic was primarily driven by the length of the bar: EJ-200 provides an optimal combination of an optical attenuation length, fast timing and high light output. The properties of EJ-200 quoted

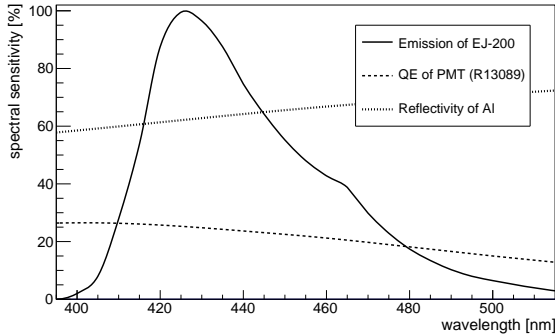


Figure 2: Emission spectrum of EJ-200 [14] (in a.u., solid line) overlaid with the quantum efficiency of the PMT [15] (dashed line) and the reflection efficiency of an aluminum foil [7] (dotted line).

by producer are: a rise time of 0.9 ns; a decay time of 2.1 ns; a bulk attenuation length of 4 m; and a refraction index of 1.58. The peak in the emission spectrum resides in the violet region of the visible spectrum. As shown in Fig. 2, this spectrum is compatible with the sensitivity region of the PMT and the reflection efficiency of an aluminum foil which was used to wrap the bar.

The bar is attached via tapered light guides to 2" phototubes on both ends. The fast Hamamatsu R13089-10 PMT [15] is chosen because of its good time resolution and moderate cost. It has a linear-focused dynode structure with 8 stages and a typical anode gain value 3.2×10^5 . Its signal output was coupled directly to the acquisition module. This results in a signal amplitude in the range 30 – 150 mV at one MIP which fits perfectly the dynamic range of the acquisition modules. The quantum efficiency of the photocathode as given by the manufacturer is 25% at the peak emission of the scintillator (see Fig. 2). Parameters relevant for the precision time measurements are a rise time of 2 ns and a transit time spread¹ of 230 ps.

We did not use an optical coupling to connect the photocathode of the PMT to the light guide. It makes possible a thin air gap between

them which may reduce the amount of photons at large angles due to total internal reflection. Furthermore, the cross-sectional area of the bar is larger than the area of the photocathode by about 34%. Due to phase-space conservation of the photon flux the light output should be reduced by about the same amount, for the case when an interaction took place in the proximity of the PMT. Both effects described in this paragraph can contribute to light reflection thus enhancing the signal in the PMT at the opposite side of the bar.

The bar and PMTs were fixed to an aluminum frame which could be moved vertically and horizontally with respect to the beam.

2.2. Beam and trigger system

Measurements were carried out using a 10 GeV/c muon beam produced by interactions of 14 GeV/c protons from the CERN PS accelerator with closed shutters at the T9 beamline of the East Hall.

The trigger was formed by the coincidence of signals from two beam counters installed 50 cm up- and downstream with respect to the bar under test as shown in Fig. 1. The counters are shaped as cubes with 2 cm sides made of a fast EJ-228 scintillator with rise and decay constants 0.5 ns and 1.4 ns, respectively. They were coupled to 1" PMTs (Philips Xp2972) from two sides via 5 cm long light guides.

The trigger time is calculated as an average of the measurements of all four trigger PMTs. This time is used as a reference for the measurement of the counter under test. The resolution of the trigger system is determined by subtracting time measurements of up- and downstream counters. It is found to be 40 ps rms. This value and the uncertainty associated with a finite size of the beam counters are subtracted in quadrature from the resolution obtained with the counter under test.

¹A spread of fluctuations of the transit time for a single photoelectron [15].

3. DAQ electronics

The major design criterion for the DAQ system is an internal time resolution which has to be much better than the expected resolution of the scintillator counter. The chosen electronics modules WAVECATCHER [12] and SAMPIC [13] are based on waveform digitizer ASICs which have been developed by LAL and IRFU teams since 1992. The technology employs a circular buffer, based on arrays of switched capacitors (SCA) which record an analog signal at very high rate. The time information is extracted with an interpolation of samples in the leading edge of the signal which permits reaching a timing accuracy of about 5 ps rms. Fast detectors for time-of-flight measurements thus represent a natural target of these digitizers. In addition they can be used for the pile-up rejection.

In both modules, common clock and trigger signals can be provided externally. Besides that, each channel also integrates a discriminator that can trigger individually or participate in a more complex trigger. This capability makes these digitizer modules very suitable for a test bench experiment since an extra electronics for trigger is not required. The digitizers combine in a single module the functions of TDC and ADC, and permit performing a digital CFD which, in case of WAVECATCHER, is a part of the firmware.

The desktop versions of the acquisition modules have been used. They house the USB2 interface which permits a connection to PC with a 480 Mbit/s speed. The acquisition softwares run on PC under Windows saving data directly on disk.

The analog signal sampling in *WAVECATCHER* is based on the SAMLONG SCA developed since 2010 [12]. The chip was designed with the AMS CMOS 0.35- μ m technology and houses two fully differential channels. The bandwidth of 500 MHz suits well for detection of very short pulses. An analog signal is sampled at a rate which can be set between

0.4 and 3.2 GS/s. Voltages stored in capacitors are further digitized with commercial ADCs at a much lower rate (10 to 20 MHz). This results in an overall readout dead time of about 120 μ s for the full sampling depth of the circular buffer which comprises 1024 cells. However one can define for the readout an interval of interest which can be a subset of the whole channel. The board is DC-coupled with dynamic range of 2.5 V and adjustable offsets are coded over 16 bits. In the acquisition of data presented in this article the desktop module with 8 channels running at 3.2 GS/s has been used.

The *SAMPIC* acquisition module is based on the cognominal ASIC designed to be the first TDC directly working on analog signals [13]. SAMPIC was developed in the frame of the R&D project aiming at a Waveform and Time to Digital Converter (WTDC) multichannel chip. It was initially intended to address needs for high precision timing detectors (5 ps rms) required by ATLAS AFP and SuperB FTOF.

SAMPIC is a 16-channel ASIC designed with the AMS CMOS 0.18- μ m technology. Each channel associates a DLL-based TDC providing a raw time with a 64-cell ultra-fast analog memory sampling up to 10.2 GS/s thus assuring the high resolution timing information. Analog data are digitized by an on-chip ADC (8 to 11 bits). The relatively small sampling depth allows for a low deadtime around 1.5 μ s when using the ADC in the 11-bit mode and of the order of 0.2 μ s in the 8-bit mode. The chip has been designed to offer a signal bandwidth of 1.5 GHz and a usable dynamic range of 1 V.

In the work presented in this paper SAMPIC was exploited at the sampling rate 3.2 GS/s. The typical length of a signal in the scintillator counter is 50 ns, thus SAMPIC would not be able to record the full signal waveform but the sampling depth of 20 ns is enough to determine the baseline and cover the front edge of the signal. The sampling rate, in general, can be lowered to 1.6 GS/s thus increasing the time

window by a factor of two.

Each channel of SAMPIC integrates a discriminator which, contrary to WAVECATCHER, can trigger itself independently of other channels. This mode was used in the data taking. Coincidence of reference counters has been checked offline and selects about 1% of recorded events. The rest of data represents a muon pile-up and cosmics.

4. Analysis

The time resolution of the counter is studied using either WAVECATCHER or SAMPIC as a function of the position of the signal in the bar (both longitudinally and transversely) and angle of incidence of the particle trajectory (with respect to both horizontal and vertical planes). The counter was exposed to the muon beam to collect about two thousand triggers for every point, after which the bar was manually either shifted or rotated to the next position. Measurements were done for 15 points along the x -axis of the bar². For each of these, two measurements were made, one at $y = 0$ cm, and one at the edge, $y = 4$ cm. Rotations were performed only for a beam position at the center of the bar, with 8 different angles between 40° and 90° in the horizontal plane and three different angles between 60° and 90° in the vertical plane.

There are several techniques for the extraction of time from the sampled waveforms [16]. However it was shown that results obtained with the digital constant fraction discrimination (dCFD) technique provides the best time resolution [17, 18]. In the dCFD approach the signal time is determined by the crossing point of the interpolated digitized signal at the threshold which, in turn, is a constant fraction of the pulse amplitude.

²Two extra points at $x = 2$ cm and $x = 298$ cm at $y = 0$ cm have been taken at the end of the run with WAVECATCHER.

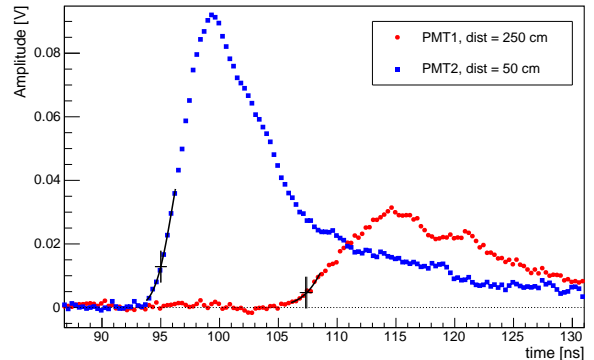


Figure 3: Typical waveforms of a signal detected by PMT1 and PMT2 and recorded by WAVECATCHER at $x = 250$ cm. Crosses show the signal time at 0.14 fraction of the pulse amplitude.

The variance of time measurements can be expressed as [18]

$$\sigma_t^2 = \left(\frac{\sigma_u}{du/dt} \right)^2 + Const \quad (1)$$

where σ_u is the variance of the measured voltage and du/dt is the slope of the rising edge of a signal. $Const$ is an uncertainty due to the limited precision of measurements (for instance the TDC jitter) which is independent of a signal.

The waveforms of a typical signal detected by PMT1 and PMT2 at $x = 250$ cm and recorded by WAVECATCHER are shown in Fig. 3. Two methods are applied to determine the crossing point of dCFD. In the first method the linear interpolation between two neighboring samples is utilized. In the second method an analytic function is used to fit the part of the waveform which includes eight consecutive samples. The second method can give an advantage in case of a long propagation of a signal along the bar, leading to a smaller number of detected photons. Indeed, if σ_u is dominated by statistical fluctuations the fit can improve the precision. If the signal propagation distance is short and, in turn, the statistical contribution to σ_u is smaller the correlation effect between samples [18] negates the improvement due to the fit, leading to no significant differ-

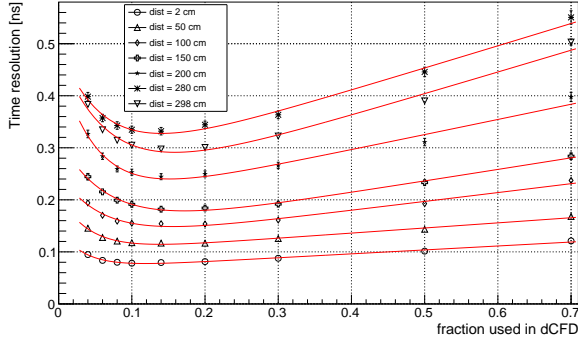


Figure 4: Time resolution of the counter as viewed by PMT1 as a function of the fraction used in dCFD. The different sets of points correspond to different distances between the interaction position and the PMT.

ence between the two methods.

The dCFD fraction should be chosen as a compromise between increasing fluctuations of the rising amplitude and improving steepness of slope (see Eq. 1). To determine the optimal fraction a scan is performed in the interval $0.04 - 0.7$. The time resolution of the counter as viewed by PMT1 as a function of the dCFD fraction is shown on Fig. 4. The value depends weakly on the distance between the interaction point and the PMT. For the analysis presented in this work 0.14 is chosen. This fraction is indicated by crosses on top of the graphs in Fig. 3.

5. Results

The dependency of the measured time versus position of the crossing point along the bar as viewed by both PMTs is shown in Fig. 5. The graphs are approximated by a polynomial of the first order. The line slope represents the effective speed of light along the x -axis of the bar, which is 16.1 cm/ns. Using the refraction index of the plastic one can convert this value to the effective average reflection angle $\langle \theta \rangle = 32.1^\circ$. Yet, observant eyes would reveal a systematic trend in the position of the points with respect to the linear function. In order to understand it we calculate the velocity and the reflection angle for every point with

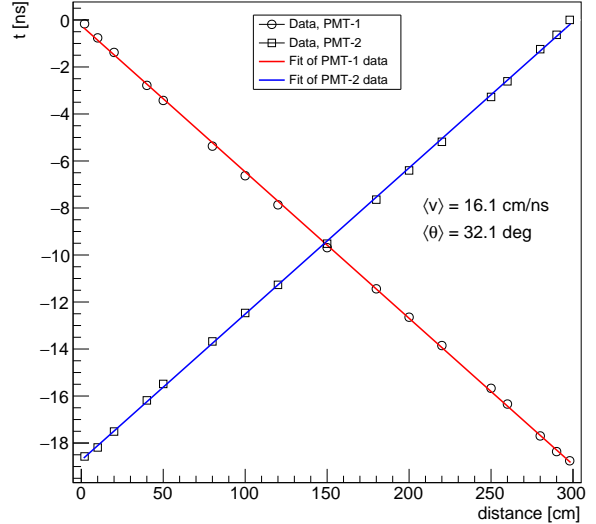


Figure 5: Time as measured by PMT1 and PMT2 as a function of the interaction position along the bar.

respect to the first measured point. Results are shown in Figs 6 and 7. The velocity of the signal propagation in the proximity of the PMT is 14 ns/cm ($\theta = 43^\circ$). It increases up to 16 ns/cm ($\theta = 33^\circ$) at $x = 180$ cm and stays rather unchanged till the end of the bar. This behavior results from a combination of multiple effects: contribution of refractive photons which, as opposed to reflective photons, enlarge the rising edge of a signal [7]; broadening of the signal due to propagation; and walk effect which however is small since CFD technique has been applied.

Time resolution was obtained in the gaussian fit of a distribution of the PMT1 and PMT2 time with the trigger time t_{ref} subtracted. The time resolution as a function of longitudinal distance at $y = 0$ cm obtained in measurements with WAVECATCHER is shown in the left panel of Fig. 8. The time of dCFD has been extracted in the fit of a waveform as described in the previous section. An advantage of this method is demonstrated in Fig. 9 which shows the ratio of resolutions obtained in the dCFD analysis of the waveform by a fit and by a linear interpolation of samples. The former provides better precision by 2% in the proximity of

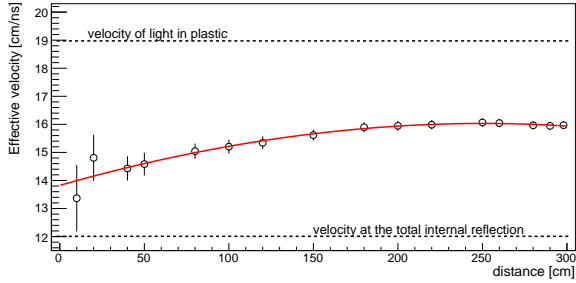


Figure 6: The effective average signal velocity along the x -axis as a function of position as viewed by PMT1.

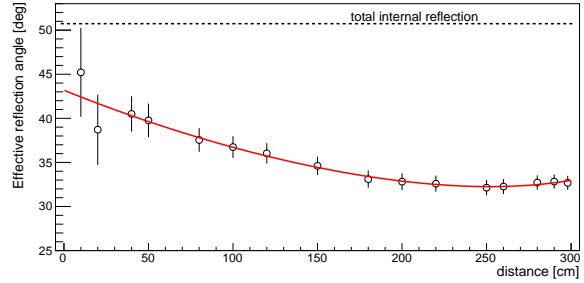


Figure 7: The effective average reflection angle as a function of position along the bar as viewed by PMT1.

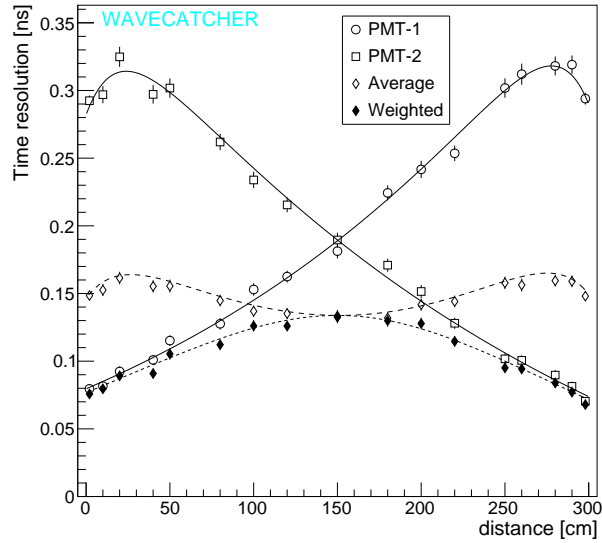


Figure 8: Time resolution as a function of a distance obtained in measurements with WAVECATCHER (left) and SAMPIC (right), resulting from a dCFD analysis exploiting a fit to determine the crossing point. The counter resolution obtained using a simple average and a weighted average of the signals from the two PMTs are also shown. Solid curves represent results of the empirical fit of an individual PMT. They are used to calculate parameters of the dashed curves which correspond to the average resolutions.

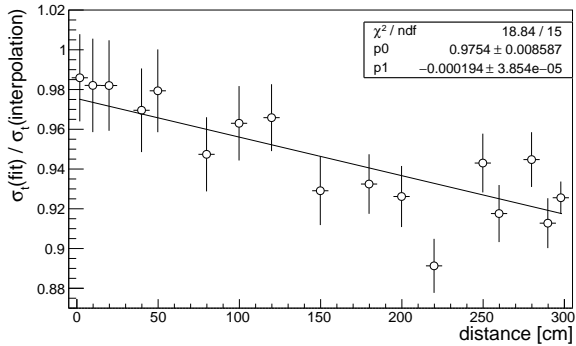
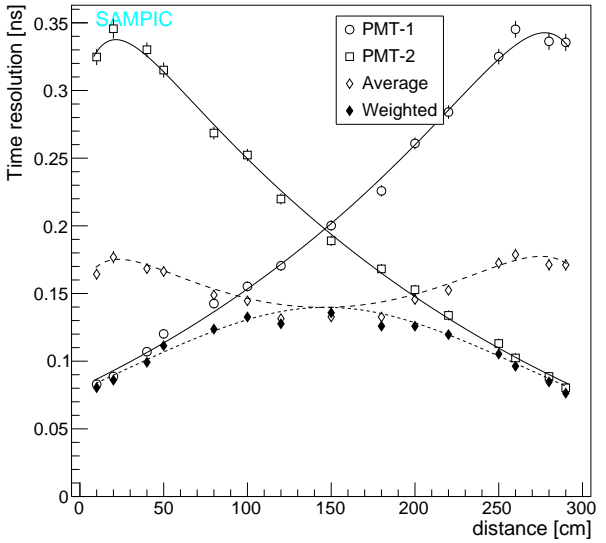


Figure 9: Ratio of the time resolution obtained in a fit and in a linear interpolation of samples used by dCFD technique. Data have been recorded by a single PMT. The line represents a fit by a first order polynomial.

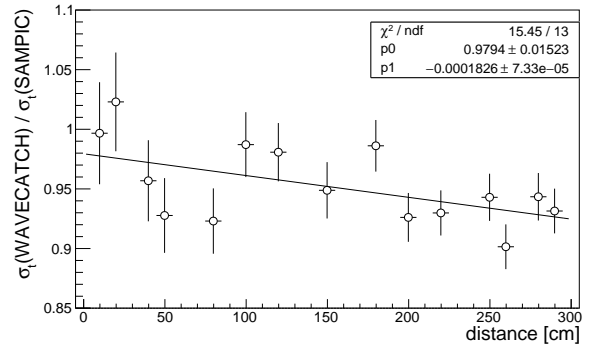


Figure 10: Ratio of the time resolution obtained in the dCFD analysis of a single PMT with data acquired by WAVECATCHER and with SAMPIC. The line represents a fit by a first order polynomial.

PMT, however an advantage becomes obvious in the outer side of the bar where the precision improves by 8%. The contribution from the reference counters is subtracted in quadrature.

The time resolution of an individual PMT evolves from 80 ps for the crossing point near the phototube to 320 ps for the light propagation along the 280 cm distance. An improvement of the resolution, in case of the crossing point approaching the end of the bar at 300 cm, is likely an effect of a signal strengthening due to the reflection (see Sec. 2.1). Similar effect was observed in Ref.[4]. The distribution is fitted by an analytic function (sum of two exponential functions and a constant) which is shown by a solid curve in Fig. 8. The physics motivated analysis of the distribution will be presented in Sec. 5.2.

In case when an information on the position of the crossing point was not used, the time of the interaction was calculated as a simple average

$$t_{aver} = \frac{t_1 + t_2}{2} \quad (2)$$

where t_1 and t_2 are the time measured by PMT1 or PMT2, respectively, with t_{ref} subtracted. However in a real experiment the crossing point can be well determined by other precision detectors. In our case the interaction point is defined by the position of the reference counters. Therefore one can weight the time measured by PMT1 or PMT2 according to their uncertainties σ_1 and σ_2

$$t_{weight} = \frac{t_1/\sigma_1^2 + t_2/\sigma_2^2}{1/\sigma_1^2 + 1/\sigma_2^2} \quad (3)$$

The counter time resolutions extracted in the gaussian fit of the distribution obtained with Eq. (2) and Eq. (3) are shown in Fig. 8 by open and full diamond symbols, respectively. Both approaches provide a precision of 133 ps in the central region of the bar. On the other hand, in the outer parts of the bar the phototube which is closer to the crossing point assures a substantially better resolution. In this region

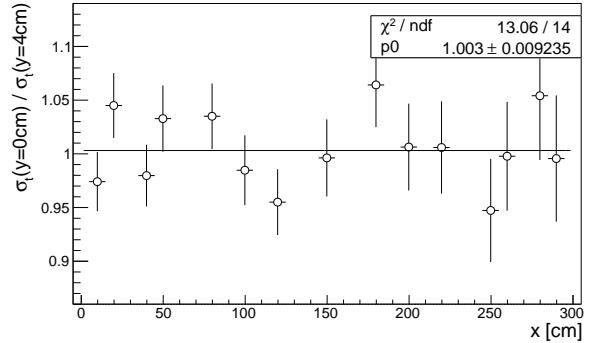


Figure 11: Ratio of time resolutions obtained in scans at $y = 0$ cm and $y = 4$ cm for PMT2. The line represents a fit by a constant.

the weighted average provides a significant advantage, with a time resolution of 80 ps, while the resolution of the simple average is around 160 ps. Therefore, the intrinsic time resolution of the counter can be regarded as being 150 ps for the simple average and 100 ps for the weighted average approach over the entire counter length of 3 m.

The time resolution as a function of longitudinal distance at $y = 0$ cm obtained in measurements with SAMPIC is shown in the right panel of Fig. 8. The time resolution of the counter when measured by a single PMT varies from 80 ps to 340 ps. The resolution in the center of the bar, when calculated as an average for two PMTs, is found to be 140 ps. The slight differences in the values obtained with SAMPIC and with WAVECATCHER could be, in general, a consequence of a shorter waveform recorded. The ratio of the two is shown in Fig. 10.

5.1. Resolution vs transverse coordinate

The time resolution of the counter was studied as a function of y . In addition to the scan at $y = 0$ cm, which is described above, a second scan with the position of trigger counters shifted by 4 cm upward was performed.

The ratio of time resolutions obtained in scans at $y = 0$ cm and $y = 4$ cm for PMT2 is shown in Fig. 11. A fit with a constant func-

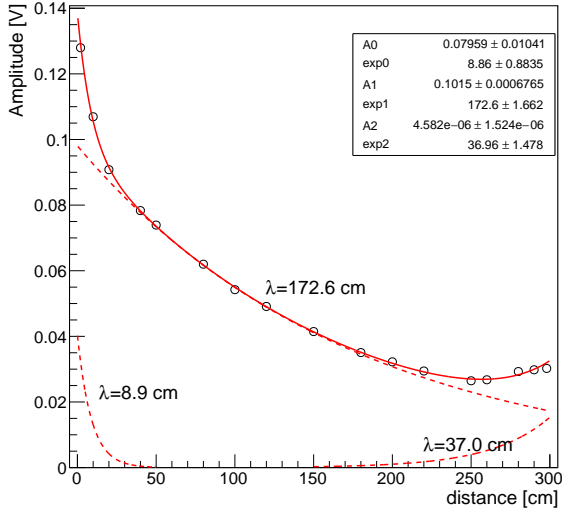


Figure 12: Average amplitude of a signal as a function of distance. The circles represent data and the solid curve shows the result of the fit by a sum of 3 exponential functions. Different contributions are shown as dashed lines.

tion gives a value compatible with 1, showing that the shift does not alter the time resolution.

5.2. Phenomenological analysis

In order to quantify the effects discussed above, a phenomenological analysis is performed aiming to describe the resolution σ_t in terms of different contributions.

The time resolution as a function of distance x can be decomposed as [19, 3]

$$\sigma_t(x) = \sqrt{\frac{\sigma_{pl+PMT}^2}{N(x)} + \frac{(\sigma_{length} \cdot x)^2}{N(x)} + \sigma_{el}^2} \quad (4)$$

where the parameter σ_{pl+PMT} represents a contribution from the emission time of the scintillator and the time jitter of the PMT; σ_{length} accounts for a time spread due to the light transmission; and σ_{el} is the contribution which is independent of the light strength, such as readout electronics noise. The number of observed photoelectrons N depends on distance and can be directly extracted in the experiment.

The signal amplitude is shown in Fig. 12 as a function of distance. One can distinguish three

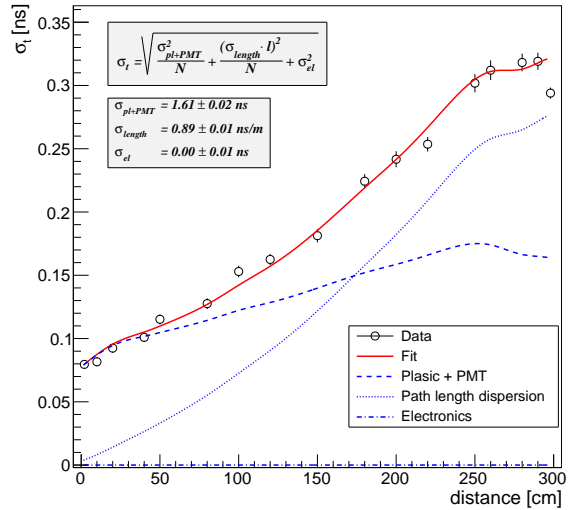


Figure 13: Time resolution as a function of distance. The circles represent data and the solid curve shows the result of the phenomenological fit. Different contributions are shown as lines of different styles.

regions, motivating a fit with a sum of three exponential functions. The distribution falls down quickly along the first 20 cm. It could be explained by the contribution of light reflected from the aluminum foil which weakens quickly with distance since in every reflection about 40% of the light is lost (see Fig. 2). Photons which undergo the total internal reflection travel a much longer distance along the bar. An angle between their trajectories and the surface of the bar has to be smaller than 51° (see Fig. 7). They make the principal contribution to the light transmission in the bar. When fitting by an exponent one obtains the effective attenuation length $\lambda_N = 172.6$ cm. Finally, when an interaction takes place at the far end of the bar reflection effects give an additional contribution to the strength of the signal.

In order to convert the amplitude into the number of photoelectrons N , we assume that they are proportional. Thus the asymmetry of amplitudes of signals detected in PMT1 and PMT2 would be equal to the asymmetry of the number of photoelectrons. The asymmetry was calculated on an event-by-event basis.

Its distribution exhibits a Gaussian shape and its spread provides the total number of photoelectrons detected in both phototubes

$$A = \frac{N_1 - N_2}{N_1 + N_2}, \quad \sigma_A \simeq \frac{1}{\sqrt{N_1 + N_2}}.$$

When calculated in the center of the bar, the procedure results in $N_1 = N_2 = 132$. This value is used to convert the distribution of amplitude to that of photoelectrons on which the fit of the time resolution σ_t with the function of Eq. (4) is performed.

The distribution of the time resolution for PMT1 overlaid with the fitting function is shown in Fig. 13. At short distance the resolution is driven by the photoemission properties of the plastic. The value obtained in the fit $\sigma_{pl+PMT} = 1.61 \pm 0.02$ ns is compatible with the time constants of EJ-200 quoted in Section 2.1. The PMT also contributes to this uncertainty via the transit time spread but at a much lower level. In the middle of the bar the contribution of the path length dispersion gets equal in size with the plastic uncertainty. This contribution is linear in distance and it enlarges the uncertainty as $\sigma_{length} = 0.89 \pm 0.01$ ns/m. The last term which reflects the contribution from the readout electronics is negligible, $\sigma_{el} = 0.00 \pm 0.01$ ns.

The fit is able to describe reasonably the time resolution except for one point at the largest distance to the PMT. This can be due to focusing effects of the reflected light from the nearest lightguide and PMT (as mentioned in Section 2.1) leading to a narrower time spread, which is not accounted for by the model.

5.3. Resolution vs incident angle

We also studied the behavior of σ_t as a function of the angle between the surface of the bar and the beam trajectory. To do so the counter was rotated in either the horizontal or the vertical plane. The time was calculated as an average between measurements of the two PMTs at the center of the bar. Results are presented in Fig. 14.

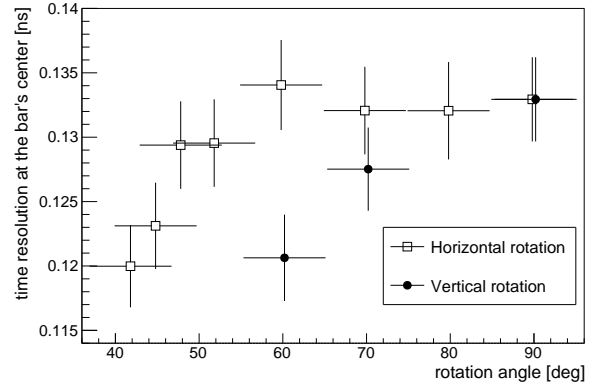


Figure 14: Time resolution at the center of the bar ($x = 150$ cm) for various angles of incidence with respect to the bar surface. Circles correspond to a bar rotation in the vertical plane while squares represent a rotation in the horizontal plane.

There are two effects which can be discussed in this respect. The track length inside the plastic gets longer in case of the oblique incidence, thus the number of emitted photons increases proportionally and the time resolution improves as a square root of this number. Indeed the measurements follow a $\sqrt{\sin \phi}$ behavior for a rotation in the vertical plane. In case of a rotation in the horizontal plane, an additional uncertainty comes from the fact that the entrance and exit points of a track are located at different distances from the PMT. As it can be seen in Fig. 14, the resolution does not change in the interval from 50° to 90° , which is in general agreement with observation presented in Refs [4, 7]. However at smaller angles the resolution improves.

6. Conclusions

The timing properties of a plastic scintillator counter with dimensions $3\text{ m} \times 11\text{ cm} \times 2.5\text{ cm}$ were studied using the test-beam facility of the East Area of the CERN PS. Two waveform digitizers, WAVECATCHER and SAMPIC, were exploited as a DAQ electronics.

The time resolution of the counter when measured by a single PMT varies from 80 ps to 320 ps and from 80 ps to 340 ps in case of

WAVECATCHER and SAMPIC, respectively and its behavior as a function of distance can be reasonably modeled. The resolution in the center of the bar, when calculated as the average of the two PMTs, is found to be 133 ps and 140 ps for the two DAQ modules, respectively. Results of measurements along the central line ($y = 0$ cm) of the bar and shifted transversely by 4 cm show no visible difference in the time resolution. The behavior of the time resolution versus incident angle in horizontal and vertical planes was also studied and the difference between the two is understood.

These results confirm that the use of long scintillator counters can provide a time resolution of approximately 100 ps for a large-scale detector used in particle physics experiments. The SAMPIC waveform digitizer appears to be adequate for such applications, especially if a self-triggering capacity and a tolerance for high signal rates is desired.

Acknowledgments

This work was supported by the Swiss National Science Foundation. We also would like to acknowledge the contribution of FAST (COST action TD1401) for inspiring a collaboration between the engineering group and the researchers. We thank the European Organization for Nuclear Research for support and hospitality and, in particular, the operating crews of the CERN PS accelerator and beamlines who made the measurements possible.

References

- [1] R. Bertoni, et al., The design and commissioning of the MICE upstream time-of-flight system, *Nucl. Instrum. Meth.* A615 (2010) 14–26. [arXiv:1001.4426](https://arxiv.org/abs/1001.4426), doi:10.1016/j.nima.2009.12.065.
- [2] K. Ahmet, et al., The OPAL detector at LEP, *Nucl. Instrum. Meth.* A305 (1991) 275–319. doi:10.1016/0168-9002(91)90547-4.
- [3] R. Perrino, et al., Timing measurements in long rods of BC408 scintillators with small cross-sectional sizes, *Nucl. Instrum. Meth.* A381 (1996) 324–329. doi:10.1016/S0168-9002(96)00812-1.
- [4] T. Tsujita, Y. Asano, H. Hamasaki, S. Mori, K. Yusa, R. D. Kephart, Test of a 3 m long, 4x4 cm² time-of-flight (TOF) scintillation counter using 38x38 mm² fine-mesh photomultipliers in magnetic fields up to 1.5 T, *Nucl. Instrum. Meth.* A383 (1996) 413–423. doi:10.1016/S0168-9002(96)00871-6.
- [5] S. Denisov, A. Dzierba, R. Heinz, A. Klimenko, V. Samoilenko, E. Scott, P. Smith, S. Teige, Systematic studies of timing characteristics for 2 m long scintillation counters, *Nucl. Instrum. Meth.* A525 (2004) 183–187. doi:10.1016/j.nima.2004.03.043.
- [6] H. Kichimia, et al., The BELLE TOF system, *Nucl. Instrum. Meth.* A453 (2000) 315–320.
- [7] C. Wu, et al., The timing properties of a plastic time-of-flight scintillator from a beam test, *Nucl. Instrum. Meth.* A555 (2005) 142–147. doi:10.1016/j.nima.2005.09.029.
- [8] C. Bernet, et al., The COMPASS trigger system for muon scattering, *Nucl. Instrum. Meth.* A550 (2005) 217–240. doi:10.1016/j.nima.2005.05.043.
- [9] N. Abgrall, et al., NA61/SHINE facility at the CERN SPS: beams and detector system, *JINST* 9 (2014) P06005. [arXiv:1401.4699](https://arxiv.org/abs/1401.4699), doi:10.1088/1748-0221/9/06/P06005.
- [10] W. Bonivento, et al., Proposal to Search for Heavy Neutral Leptons at the SPS [arXiv:1310.1762](https://arxiv.org/abs/1310.1762).
- [11] M. Anelli, et al., A facility to Search for Hidden Particles (SHiP) at the CERN SPS [arXiv:1504.04956](https://arxiv.org/abs/1504.04956).
- [12] D. Breton, E. Delagnes, J. Maalmi, P. Rusquart, The WaveCatcher Family of SCA-Based 12-Bit 3.2-GS/s Fast Digitizers, RT2014 - 19th Real-Time Conference, poster (May 2014). URL <http://hal.in2p3.fr/in2p3-00995691>
- [13] E. Delagnes, D. Breton, H. Grabas, J. Maalmi, P. Rusquart, M. Sainpert, The SAMPIC Waveform and Time to Digital Converter, in: 2014 IEEE Nuclear Science Symposium and Medical Imaging Conference (2014 NSS/MIC), Seattle, United States, 2014, sce Electronique. URL <http://hal.in2p3.fr/in2p3-01082061>
- [14] SCIONIX HOLLAND BV, Radiation Detectors & Crystals, <http://scionix.nl>.
- [15] Hamamatsu, <http://www.hamamatsu.com>.
- [16] M. Nelson, B. Rooney, D. Dinwiddie, B. G., Analysis of digital timing methods with BaF₂ scintillators, *Nucl. Instrum. Meth.* A505 (2003) 324–327. doi:10.1016/S0168-9002(03)01078-7.
- [17] J. Wang, S. Liu, Q. An, Waveform Timing Performance of a 5 GS/s Fast Pulse Sampling Module with DRS4, *Chin. Phys. C39* (10) (2015) 106101. [arXiv:1501.00651](https://arxiv.org/abs/1501.00651), doi:10.1088/1674-1137/39/10/106101.

- [18] E. Delagnes, What is the theoretical time precision achievable using a dCFD algorithm? [arXiv:1606.05541](https://arxiv.org/abs/1606.05541).
- [19] M. Kuhlen, M. Moszynski, R. Stroynowski, E. Wicklund, B. Milliken, Timing properties of long scintillation counters based on scintillating fibers, *Nucl. Instrum. Meth.* A301 (1991) 223–229. [doi:10.1016/0168-9002\(91\)90463-Z](https://doi.org/10.1016/0168-9002(91)90463-Z).